MDPI

*Article*

# New Radical Cation Salts Based on BDH-TTP Donor: Two Stable Molecular Metals with a Magnetic [ReF$_6$]$^{2-}$ Anion and a Semiconductor with a [ReO$_4$]$^-$ Anion

Nataliya D. Kushch [1,*], Gennady V. Shilov [1], Lev I. Buravov [1], Eduard B. Yagubskii [1,*], Vladimir N. Zverev [2,3], Enric Canadell [4] and Jun-ichi Yamada [5]

[1] Institute of Problems of Chemical Physics RAS, 142432 Chernogolovka, Russia; shilg@icp.ac.ru (G.V.S.); buravov@icp.ac.ru (L.I.B.)
[2] Institute of Solid State Physics, Russian Academy of Sciences, 142432 Chernogolovka, Russia; zverev@issp.ac.ru
[3] Moscow Institute of Physics and Technology, 141700 Dolgoprudnyi, Russia
[4] Institut de Ciència de Materials de Barcelona (ICMAB-CSIC), Campus de la U.A.B., E-08193 Bellaterra, Spain; canadell@icmab.es
[5] Department of Material Science, Graduate School of Material Science, University of Hyogo, 3-2-1 Kyoto, Kamigori-choAko-gun, Hyogo 678-1297, Japan; yamada@sci.u-hyogo.ac.jp
* Correspondence: kushch@icp.ac.ru (N.D.K.); yagubski@gmail.com (E.B.Y.)

check for updates

**Abstract:** Three radical cation salts of BDH-TTP with the paramagnetic [ReF$_6$]$^{2-}$ and diamagnetic [ReO$_4$]$^-$ anions have been synthesized: κ-(BDH-TTP)$_4$ReF$_6$ (**1**), κ-(BDH-TTP)$_4$ReF$_6$·4.8H$_2$O (**2**) and pseudo-κ″-(BDH-TTP)$_3$(ReO$_4$)$_2$ (**3**). The crystal and band structures, as well as the conducting properties of the salts, have been studied. The structures of the three salts are layered and characterized by alternating κ-(**1**, **2**) and κ″-(**3**) type organic radical cation layers with inorganic anion sheets. Similar to other κ-salts, the conducting layers in the crystals of **1** and **2** are formed by BDH-TTP dimers. The partial population of positions of Re atoms and disorder in the anionic layers of **1–3** are their distinctive features. Compounds **1** and **2** show the metallic character of conductivity down to low temperatures, while **3** is a semiconductor. The *ac* susceptibility of crystals **1** was investigated in order to test the possible slow relaxation of magnetization associated with the [ReF$_6$]$^{2-}$ anion.

**Keywords:** organic conductors; metal complex anions; molecular magnets; electrocrystallization; crystal and band structures; conductivity; magnetic properties

## 1. Introduction

Multifunctionality is one of the most attractive trends in the chemistry of modern materials. Among multifunctional materials, compounds combining electrical conductivity and magnetism in the same crystal lattice have been the object of intense study in recent decades [1–6]. This interest is associated with the search for synergy of these properties, which can lead to new phenomena and the tuning of one of the properties as a response to an external factor affecting the other. Research in this area is focused mainly on the family of quasi-two-dimensional (super)conductors based on the radical cation salts of bis(ethylenedithio)tetrathiafulvalene (BEDT-TTF, Scheme 1) and its derivatives with various paramagnetic metal complex anions. In such compounds, the electrical conductivity is associated with mobile electrons of the organic layers, and transition metal ions in the insulating anion layers are responsible for magnetism. Among the possible magnetic counterions for conducting radical cation salts, molecular nanomagnets—the so-called single molecular magnets (SMMs)—attract much attention. SMMs exhibit unique magnetic properties at liquid helium temperatures such as slow magnetization relaxation, blocking and quantum magnetization tunneling and, due to these properties, the SMMs are promising compounds [7–11]. The creation of multifunctional compounds combining conductivity

and single molecule magnetism could open new directions in terms of further studying the fundamental properties and practical applications of molecular nanomagnets. In particular, the study of the relationship between relaxing local spins and conducting electrons in superparamagnetic/conducting hybrid materials is important for the development of quantum spintronic systems.
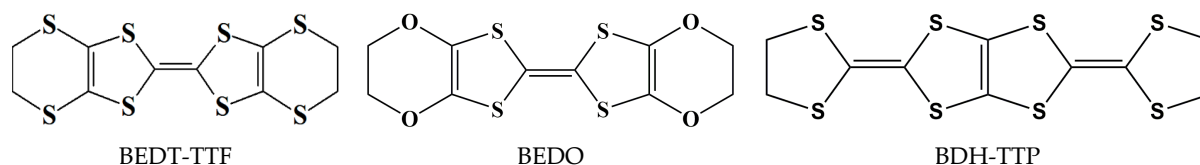


**Scheme 1.** $\pi$-donor molecules.

There are already several publications in the literature devoted to the design and synthesis of conducting radical anion salts based on the $M(dmit)_2$ complexes and tetra-cyanoquinodimethane containing cationic metal complexes as counterions, showing slow magnetic relaxation [6,12,13]. Recently, a radical cation salt of BEDT-TTF has also been synthesized with a single-molecule magnet as a counterion, namely, an anionic trifluoroacetate dysprosium complex [14]. However, in all these compounds, conductivity and single-molecule magnetism occur in different temperature ranges: the single-molecule magnetic properties appear at very low helium temperatures (usually below 20 K), while the conductivity is at best maintained up to the liquid nitrogen (77.2 K). In 2018, we used the oxygen analog of BEDT-TTF, bis(ethylenedioxo)tetrathiafulvalene (BEDO), Scheme 1, as an organic $\pi$-donor and investigated its electrochemical oxidation in the presence of the Re(IV) hex-afluoride complex, $[ReF_6]^{2-}$, which in the composition of $(PPh_4)_2[ReF_6]\cdot 2H_2O$ salt displays SMM properties below 5 K under application of a low permanent magnetic field [15]. As a result, the first conductive field-induced SMM was synthesized—$(BEDO)_4[ReF_6]\cdot 6H_2O$—in which conductivity and single-molecule magnetism coexist in the same temperature range [16]. More recently, another BEDO salt has been synthesized with a monomolecular magnet $[Co(pdms)]^{2-}$ as a counterion, which also shows the coexistence of conductivity and monomolecular magnetism up to 11 K [17].

In the present work, we investigated the electrochemical oxidation of 2,5-bis (1,3-dithiol-2-ylidene)-1,3,4,6-tetrathiapentalene donor, $C_{10}S_8H_8$, (BDH-TTP, Scheme 1) in the presence of $(PPh_4)_2[ReF_6]$ $2H_2O$, electrolyte. Our choice of the BDH-TTP donor, as in the case of BEDO, is determined by the fact that it forms radical cation salts with counterions of a different nature, size and shape, which retain metallic conductivity up to the temperature of liquid helium (4.2 K) [18,19].

Unlike BEDT-TTF and its derivatives, in the case of BDH-TTP and BEDO, the crystalline packing of the conducting layers is determined primarily by the nature of these donors themselves, and the counterions have almost no effect on the packing of the radical cation layers. Herein, we report the synthesis and the crystalline and band structures, as well as the transport properties under the normal and high pressure of new organic metals based on BDH-TTP, $\kappa$-(BDH-TTP)$_4$ReF$_6$ (**1**) and $\kappa$-(BDH-TTP)$_4$ReF$_6\cdot 4.8H_2O$ (**2**), containing $\kappa$-type organic layers as well as the new semiconductor, pseudo-$\kappa''$-(BDH-TTP)$_3$(ReO$_4$)$_2$ (**3**). To probe the magnetization dynamics of **1,** the ac susceptibility was studied.

## 2. Results and Discussion

### 2.1. Synthesis

Electrochemical oxidation of the BDH-TTP donor has been studied in a medium chlorobenzene (CB) + 10% abs. ethanol, (CB) + (5 ÷ 15%) rectified (96%) ethanol containing 4% water and (CB) + 10% trifluoroethanol. Different types of alcohol have been used as additives to the main solvent CB. The $(Ph_4P)_2[ReF_6]\cdot 2H_2O$ salt has been used as an electrolyte. Crystals of **1** grow when trifluoroethanol is used as an additive. In a mixture of CB with the addition of 96% ethanol, the crystals of **2** and **3** formed simultaneously at the

anode while electrocrystallization was not observed in the presence of the absolute alcohol due to the inability to set the desired current. Thus, it can be stated that alcohol additives have a decisive influence on the formation of these BDH-TTP salts. Moreover, the formation of salt **3** indicates that, in the process of electrocrystallization, $Re^{4+}$ is oxidized to $Re^{7+}$. The synthetic procedure for the preparation of salts **1–3** is given in the experimental section.

### 2.2. Crystal Structure

The prepared radical cation salts were characterized by the layered structures with alternating conductive radical cation layers and insulating anionic sheets formed with $[ReF_6]^{2-}$ octahedra in salt **1**, $[ReF_6]^{2-}$ octahedra and water molecules in **2** or $[ReO_4]^{-}$ tetrahedra in **3**. Crystallographic data and refined structural parameters for the crystals **1–3** are given in Table S1, Supplementary Materials.

2.2.1. Crystal Structure of the Salts κ-(BDH-TTP)$_4$ReF$_6$ (**1**) and κ-(BDH-TTP)$_4$ReF$_6$·4.8H$_2$O (**2**)

The compound **1** crystallizes in a monoclinic system ($P2_{1}/_C$ space group). The asymmetric part of the crystal structure consists of one molecule of BDH-TTP and one anion in the general position with a population of 0.25 (see Figure S1, ESI). Thus, there is one anion and four radical cations per unit cell. Figure 1 shows the layered structure of the crystals of **1**, in which conductive and insulating layers alternate along the *a*-axis. The radical cationic layers in **1** are packed in a typical κ-type arrangement formed by BDH-TTP equivalent dimers (Figure 2a), which are located at an angle of 83.78° relative to each other.

The donor molecules are arranged into "face-to-face" dimers by a "ring-over-bond" type (Figure S2, Supplementary Materials) [19]. This configuration, in which two neighboring donor molecules are shifted in relation to each other along the long molecular axis by approximately a length of the C=C double bond (~1.4 Å), is typical for the BEDT-TTF and BDH-TTP κ-salts [18–20]. The terminal ethylene groups in **1** are disordered. The central C=C bond length of the radical cation, as well as two terminal C=C bond lengths in the TTP fragments, have almost the same values (1,353–1.357 Å), which correspond well to the charge +0.5 [18–21]. The anionic layer, formed by isolated anions with the incomplete population of Re (Figure 2b), is highly disordered. Since it has been impossible to accurately determine the position of fluoride ions in the octahedra, they have therefore been refined with restrictions on bond lengths and thermal parameters.
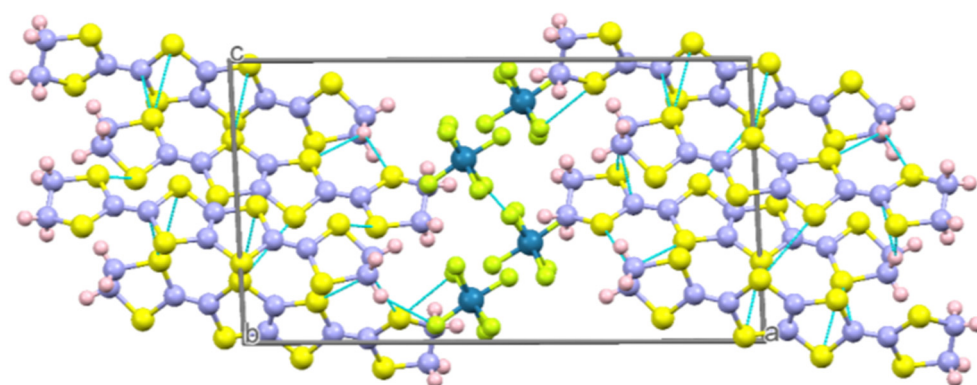


**Figure 1.** Crystal structure of the κ-(BDH-TTP)$_4$ReF$_6$ (**1**) salt projected on the *ac*-plane. Dashed lines show shortened intermolecular contacts between the BDH-TTP molecules.
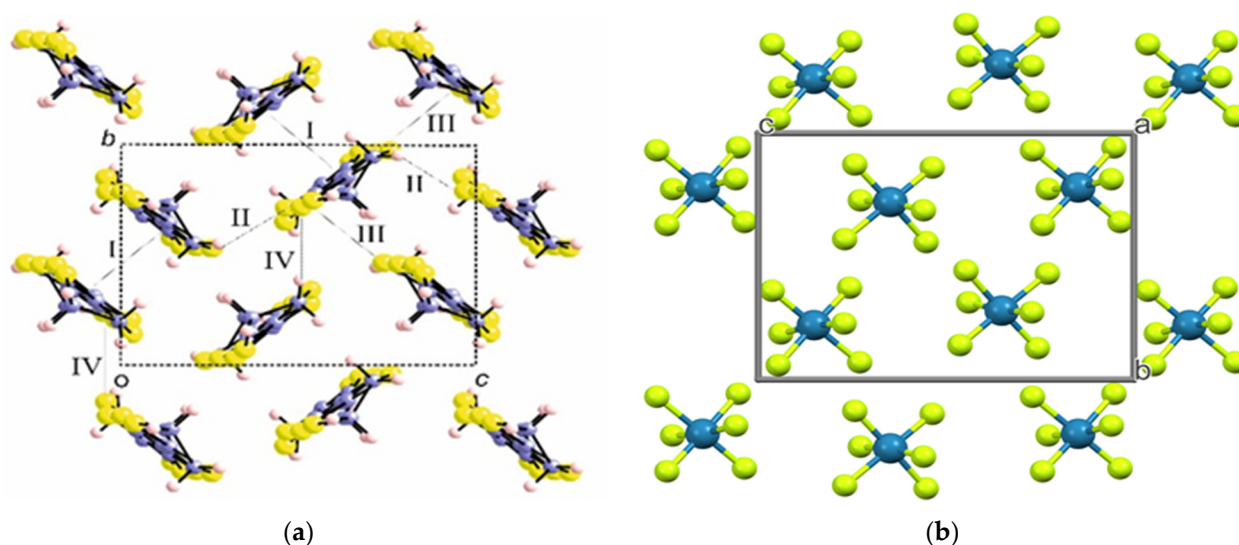
**Figure 2.** Projections of: (**a**) the radical cation layer, where the different intermolecular interactions are labeled and (**b**) the anionic layer along the *a* axis in the κ-(BDH-TTP)$_4$ReF$_6$ (**1**) salt.

Between the dimers there are four short S . . . S contacts and one short S . . . C contact, and the contacts involving hydrogen atoms (Table 1), while inside the dimers in the conducting layers, are only intermolecular contacts of the types S . . . HC (S5 . . . H9A) and C . . . HC (C6 . . . H9A).

**Table 1.** Short intermolecular contacts in the structure of the salt **1**.

| Short Contact | Contact Length, Å | Symmetry Operation for the 1st Atom in Contact |
|:---:|:---:|:---:|
| S1 . . . S2 | 3.584 | x, y, z |
| S3 . . . S1 | 3.531 | x, y, z |
| S8 . . . S3 | 3.549 | x, y, z |
| S7 . . . S5 | 3.516 | x, y, z |
| S8 . . . C5 | 3.434 | x, y, z |
| S4 . . . H10A | 2.977 | x, y, z |
| S6 . . . H10A | 2.942 | x, y, z |
| S5 . . . H9A | 2.858 | x, y, z |
| C6 . . . H9A | 2.822 | x, y, z |

Salt **2** crystallizes in a monoclinic system and, in contrast to **1**, was refined in the space group *C2/c*. The asymmetric part of the crystal structure comprises the [ReF$_6$]$^{2-}$ anion in a general position with a population of 0.25 disordered by the two-fold axis, a radical cation in a general position and three water molecules with a population of 0.72, 0.24, 0.24, respectively. Thus, there are two anions and eight radical cations per unit cell or, formally, one Re atom for four BDH-TTP molecules (see Figure S3, Supplementary Materials). Consequently, the composition of salt **2** differs from **1** by the presence of water molecules in its structure. The crystal structure of **2** is shown in Figure 3, in which conductive and insulating anionic layers alternate along the *a*- axis. The radical cation layers consist of BDH-TTP dimers built from two identical donor molecules with an average charge of +0.5 per molecule (κ-type packing) (Figure 4a). Terminal ethylene groups in the BDH-TTP radical cations are disordered.
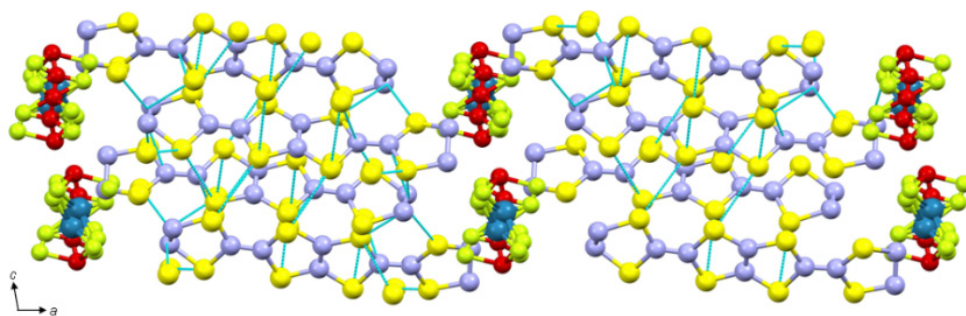
**Figure 3.** Crystal structure of the κ-(BDH-TTP)$_4$ReF$_6$·4.8H$_2$O (**2**) salt projected on the *ac*-plane. Dashed lines show shortened intermolecular contacts between the BDH-TTP molecules.
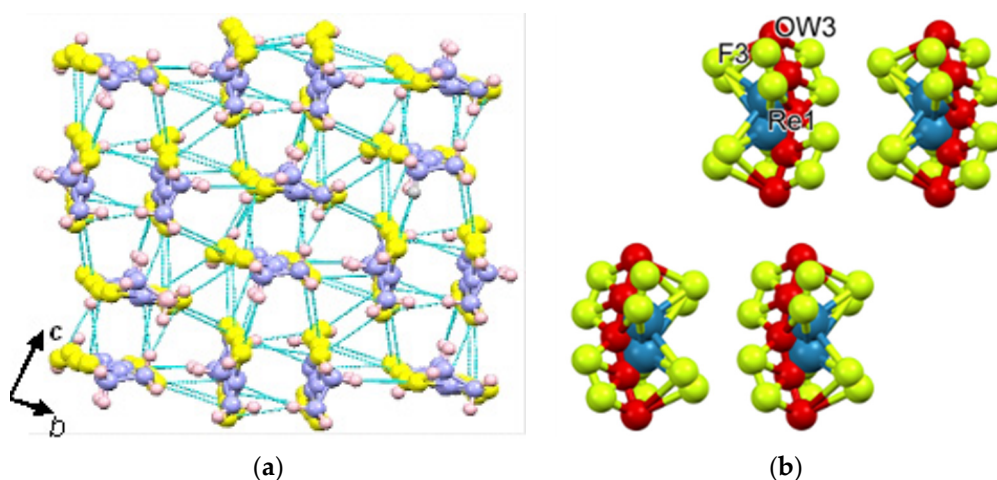


(**a**)



(**b**)

**Figure 4.** (**a**) Projection of the conducting layer on the *bc*-plane and (**b**) Optimal view of the anionic layer fragment in the κ-(BDH-TTP)$_4$ReF$_6$·4.8H$_2$O (**2**) salt.

As in salt **1**, the BDH-TTP dimers in **2** have a "ring-over-bond" configuration (Figure S4, Supplementary Materials). Inside the dimers, the central parts of the donor molecules are almost parallel. The dihedral angle between the neighboring dimers is 83.45°. As in salt **1**, this angle in **2** is smaller by ≈16° than those characteristic of classical BEDT-TTF and BETS κ-type salts [3,4,20].

The conducting layers are characterized by the presence of several short S . . . S contacts, some of which are shorter than the sum of the Van der Waals radii by 0.007–0.110 Å. In addition to these contacts there are also intermolecular contacts of the S . . . H-C and C . . . H-C types (Table 2). Between the dimers there are six short S . . . S- and one S . . . C contact and also intermolecular contacts S2 . . . HC7 and S7 . . . HC7. In the dimer, only intermolecular contacts S8 . . . H8B and C6 . . . H8B are present (Table 2).

The anionic layers of salt **2** consist of the isolated octahedral [ReF$_6$]$^{2-}$ anions and water molecules localized near them. Figure 4b shows a fragment of the anionic layer. The octahedral anions in **2** are more distorted, compared with those in **1**. As a result of significant disorder in the anionic layer, the atomic population of the [ReF$_6$]$^{2-}$ anion and water molecules have been refined with restrictions on bond lengths and thermal parameters and then fixed, as in salt **1**. As a consequence, it has not been possible to accurately analyze the different interactions leading to the actual crystal package in both salts.

### 2.2.2. Crystal Structure of the Pseudo-κ''-(BDH-TTP)$_3$(ReO$_4$)$_2$ (**3**) Salt

Radical cation salt **3** crystallizes in the triclinic system. The asymmetric unit includes the [ReO$_4$]$^-$ anion in the general position and two radical cations in the general position (Figure S5, Supplementary Materials). In the anion, oxygen atoms are disordered over two positions with occupancies 0.63 and 0.37. The radical cation and anion layers alternate

along the *c* axis of the unit cell (Figure 5). The radical cations in the conducting layers form a two-dimensional network connected by several short contacts S...S and intermolecular contacts CH...S, Figure 6a. Values of short contacts and intermolecular CH...S contacts in the structure of **3** are listed in Table 3.

**Table 2.** Short intermolecular contacts in the structure of the salt **2**.

| Short Contact | Contact Length, Å | Symmetry Operation for the 1st Atom in Contact |
|:---:|:---:|:---:|
| S3 . . . S1 | 3.569 | x, y, z |
| S2 . . . S5 | 3.581 | x, y, z |
| S4 . . . S6 | 3.537 | x, y, z |
| S4 . . . S1 | 3.531 | x, y, z |
| S3 . . . S6 | 3.593 | x, y, z |
| S5 . . . S8 | 3.490 | x, y, z |
| C5 . . . S6 | 3.416 | x, y, z |
| C7H . . . S2 | 2.057 | x, y, z |
| C7H . . . S7 | 2.878 | x, y, z |
| S8 . . . H8B | 2.957 | x, y, z |
| C6 . . . H8B | 2.782 | x, y, z |
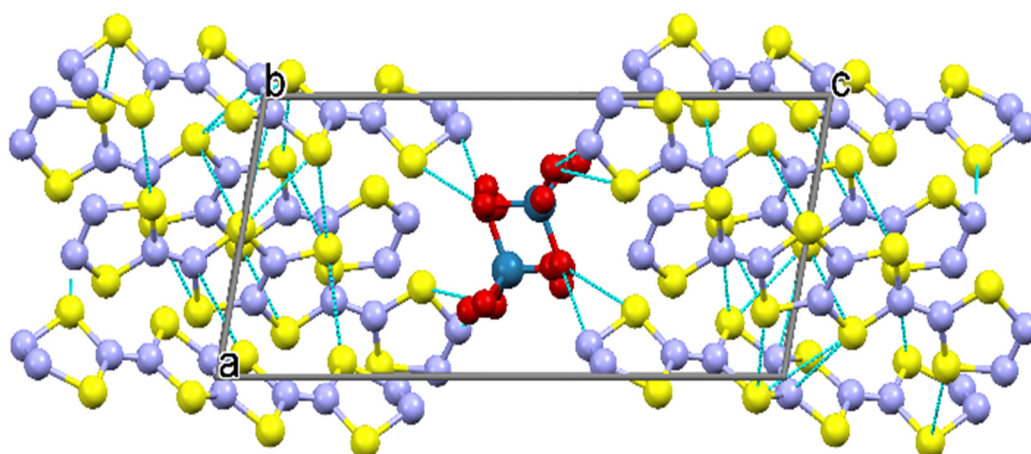


**Figure 5.** Projection of the crystal structure of the pseudo-κ''-(BDH-TTP)$_3$(ReO$_4$)$_2$ salt (**3**) on the *ac* plane; dashed lines show shortened intermolecular contacts between the BDH-TTP molecules.



(**a**)

(**b**)

**Figure 6.** (**a**) Optimal view of the radical cation layers of the salt pseudo-κ''-(BDH-TTP)$_3$(ReO$_4$)$_2$ (**3**); The single molecules BDH-TTP are highlighted by circles; (**b**)The disordered anion [ReO$_4$]$^-$ in the structure of 3 with the numbering of the atoms in the tetrahedron.

**Table 3.** The short intermolecular contact values and hydrogen bonds in the structure of salt **3**.

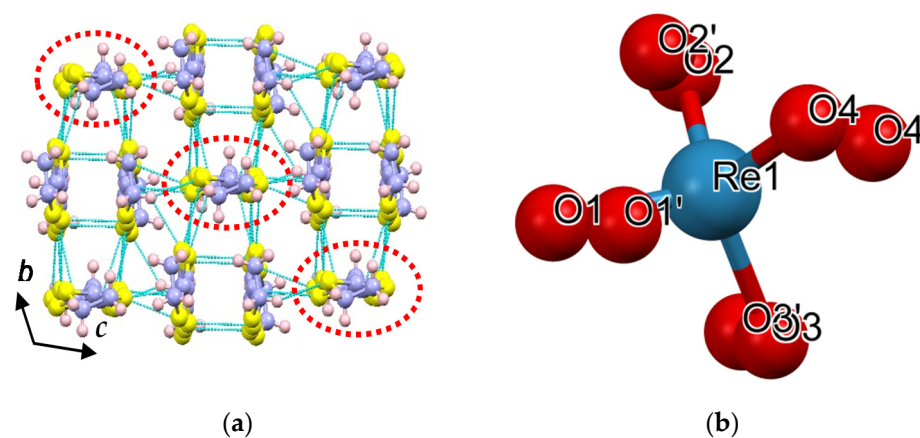| Short Cotact | Length, Å | Sym. Operation for the 1st Atom | Short Contact | Length, Å | Sym. Operation for the 1st Atom |
|---|---|---|---|---|---|
| O3 . . . S10 | 3.045 | x, y, z | S12 . . . 3 | 3.498 | x, y, z |
| O4 . . . S5 | 3.045 | x, y, z | S12 . . . S2 | 3.260 | x, y, z |
| O1 . . . C5 | 3.126 | x, y, z | S10 . . . S4 | 3.579 | x, y, z |
| O3 . . . C14 | 3.160 | x, y, z | C15 . . . S3 | 3.466 | x, y, z |
| O3 . . . C6 | 3.204 | x, y, z | S9 . . . S6 | 3.482 | x, y, z |
| O4 . . . C10 | 3.160 | x, y, z | S9 . . . C7 | 3.296 | x, y, z |
| O3 . . . C6 | 3.204 | x, y, z | S6 . . . S2 | 3.423 | x, y, z |
| O2 . . . C6 | 3.059 | x, y, z | S11 . . . S7 | 3.244 | x, y, z |
| O2 . . . H6A | 2.246 | x, y, z | S11 . . . S6 | 3.531 | x, y, z |
| O1 . . . H6A | 2.707 | x, y, z | C15 . . . S7 | 3.383 | x, y, z |
| O4 . . . H14B | 2.533 | x, y, z | S9 . . . S8 | 3.457 | x, y, z |
| O2 . . . H13A | 2.496 | x, y, z | S3 . . . S7 | 3.466 | x, y, z |
| O1 . . . H5B | 2.559 | x, y, z | S10 . . . H6B | 2.943 | −1 + x, 1 + y, z |
| O1 . . . H9A | 2.612 | x, y, z | S4 . . . H6B | 2.873 | x, y, z |

The conducting layers in **3** are built from dimers and single donor molecules (so called pseudo-κ-type packing) [5,22]. In the dimers, the radical cations are located "face-to-face" with a longitudinal shift larger than the shifts in salts **1** and **2** (Figure S6, Supplementary Materials). The pseudo-κ′-type packing, where four single molecules surround one dimer, is described in BEDT-TTF salts [5,22]. Unlike the known BEDT-TTF salts with pseudo-κ′-type packing [5,22], we have observed four dimers surrounding a donor molecule (new pseudo-κ″-type packing) in **3** (Figure 6a). This type of packing of conducting organic layers has not been previously observed in radical cation salts. The dihedral angle between the single BDH-TTP molecule and dimer is 84.45°. The distances between the radical cations in dimer and between single molecules are equal to 3.289 Å and 5.374 Å, respectively. The distances along the *a* and *b* axes between the radical cations in the dimer and a single BDH-TTP molecule are 3.456 and 3.651 Å, respectively. The lengths of C=C bonds in the single radical cation and dimer are shown in Table 4. By the value of C=C bonds, one can estimate the charge state of the BDH-TTP molecule [18,21]. From the analysis of the values of these bonds, it can be assumed that the charge state of a single BDH-TTP molecule is close to 0, and that of dimer molecules is close to +2. However, the presence of short contacts between dimers and single ET molecules (Figure S7, Supplementary Materials) indicates the existence of some charge transfer between them. In order to clarify this situation, the electronic band structure of **3** was calculated (see the electronic structures section).

**Table 4.** The lengths of C=C bonds in the dimer and single radical cation of salt **3**.

| C=C Bond in the Dimer Radical Cation | Length of C=C Bond, Å | C=C Bond in the Single Radical Cation | Length of C=C Bond, Å |
|---|---|---|---|
| central C1=C2 | 1.374 | central C15=C15 | 1.362 |
| terminal C3=C4 | 1.358 | terminal C11=C12 | 1.345 |
| terminal C7=C8 | 1.365 | terminal C11=C12 | 1.345 |

Anionic layers are formed by isolated anions $[ReO_4]^-$. Each Re atom has a tetrahedral environment and is bonded to four oxygen atoms (Figure 6b). Between the BDH-TTP molecules and $[ReO_4]^-$ tetrahedra there are short C...O and S...O contacts as well as intermolecular C-H . . . O contacts (see Table 4). The Re-O bond lengths in the tetrahedra are within the interval 1.700–1.786 Å range, Table S2, Supplementary Materials

## 2.3. Electronic Structure of the BDH-TTP Salts

### 2.3.1. Electronic Structure of κ-(BDH-TTP)$_4$ReF$_6$ (1) and κ-(BDH-TTP)$_4$ReF$_6$·4.8H$_2$O (2)

The donor layers of **1** contain only one type of BDH-TTP dimer built from two identical donors and there are four different types of HOMO . . . HOMO (highest occupied molecular orbital) intermolecular interactions (see Section 2, Figure 2a): (i) the intra-dimer interaction (I); (ii) two interactions between donors in different dimers almost orthogonal (II and III); and (iii) one interaction between donors in different dimers forming a chain along the *b*-direction (IV). The strength of these interactions can be qualified from the so-called HOMO . . . HOMO interaction energies [23]. Those calculated for the present salt are 0.3567 (I), 0.0826 (II) 0.1372 (III) and 0.2326 (IV) eV. These values implicate very similar inter-dimer interactions along the two main directions of the lattice. Thus, as far as the HOMO . . . HOMO interactions are concerned, this salt must be very isotropic within the layers plane. This was also the case with other BDH-TTP κ-type salts such as κ-(BDH-TTP)$_2$X with X = [FeNO(CN)$_5$], PF$_6$, FeCl$_4$, and [Hg(SCN)$_4$].C$_6$H$_5$NO$_2$ [18,21,24,25]. For instance, the HOMO . . . HOMO interaction energies calculated for the first of these salts are: 0.3613 (I), 0.0742 (II) 0.1476 (III) and 0.2420 (IV) eV, which are remarkably similar to those of κ-(BDH-TTP)$_4$ReF$_6$. Since the shape of the anions in these salts is quite different, it is clear that the inner structure of many BDH-TTP κ-salts is mostly determined by the intra-layer hydrogen bonding and S . . . S interactions with only a minor influence of the anions, which tend to adapt to it. The calculated band structure of **1** is shown in Figure 7a. Since the repeat unit of the donor layer contains four donors, Figure 7a contains four HOMO-based bands. With one-quarter occupation of the anion positions, the HOMO bands must contain two holes so that the Fermi level cuts the two upper HOMO bands and the system should exhibit metallic behavior, in agreement with our transport measurements.
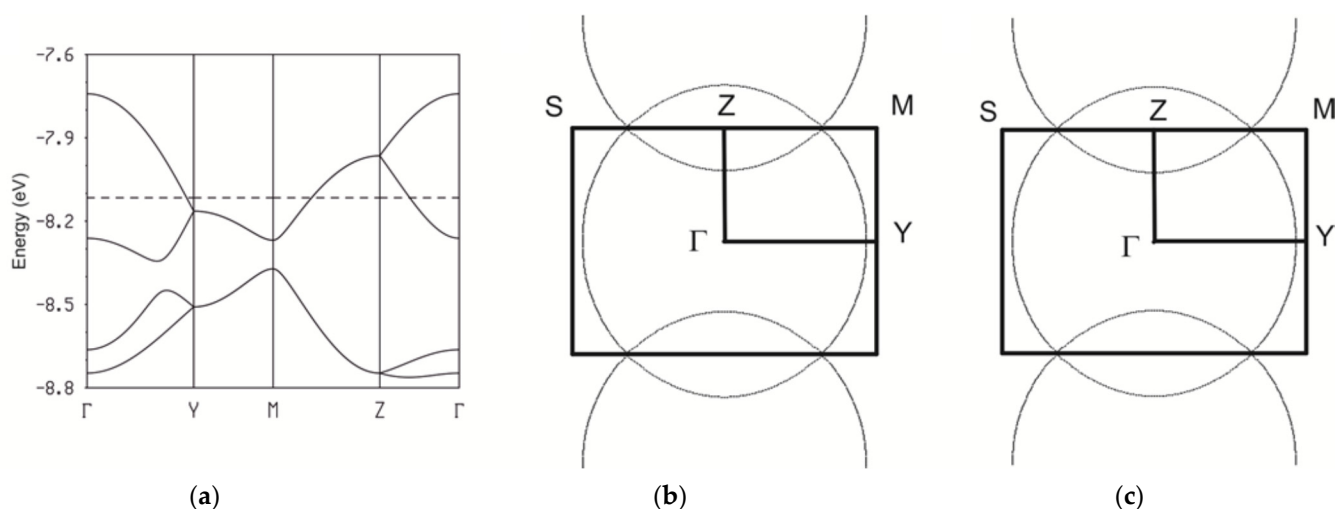


|  |  |  |
|:---:|:---:|:---:|
| (**a**) | (**b**) | (**c**) |

**Figure 7.** (**a**) Calculated band structure and (**b**) Fermi surface for the donor layers of κ-(BDH-TTP)$_4$ReF$_6$ (**1**); (**c**) Fermi surface calculated for the donor layers of κ-(BDH-TTP)$_4$ReF$_6$·4.8H$_2$O (**2**). In (**a**) the dashed line refers to the Fermi level. Γ = (0, 0), Y = (*b**/2, 0), Z = (0, *c**/2), M = (*b**/2, *c**/2) and S = (−*b**/2, *c**/2).

The calculated Fermi surface is shown in Figure 7b: it is made of a series of superposed cylinders with a practically circular cross section. The area of the large circles of Figure 7b amounts to 100% of the cross-sectional area of the Brillouin zone, whereas that of the closed circuit around Z amounts to 16.6%.

Despite the fact that the 3D crystal structure of κ-(BDH-TTP)$_4$ReF$_6$·4.8H$_2$O is different from that of κ-(BDH-TTP)$_4$[ReF$_6$], the donor layers are structurally very similar. In particular, they contain only one type of BDH-TTP dimer built from two identical donors. The calculated β$_{|HOMO-HOMO|}$ interactions energies for this salt are: 0.3536 (I), 0.0797(II) 0.1363 (III) and 0.2392 (IV) eV. These values are almost identical to those for κ-(BDH-TTP)$_4$ReF$_6$, thus confirming the small influence of the anion shape over the internal structure of the

BDH-TTP κ-type layers. This is in contrast to the situation for the κ- phases of BEDT-TTF and may be a useful guiding principle in the search for multifunctional materials. As expected from the strong similarity in HOMO . . . HOMO interactions, the electronic structure of the two salts is completely equivalent. For instance, the Fermi surface calculated for the donor layers of κ-(BDH-TTP)$_4$ReF$_6$·4.8H$_2$O is shown in Figure 7c. The area of the large circles of Figure 7c amounts to 100% of the cross sectional area of the Brillouin zone, whereas that of the closed circuit around Z amounts to 17% (to be compared with 16.6% for κ-(BDH-TTP)$_4$ReF$_6$). Thus, our study suggests that both salts could exhibit Shubnikov-de Haas oscillations of the magnetoresistance with a frequency corresponding approximately to 17% of the cross-section area of the Brillouin zone. In short, despite the different crystal structures, κ-(BDH-TTP)$_4$ReF$_6$ and κ-(BDH-TTP)$_4$ReF$_6$·4.8H$_2$O are almost indistinguishable.

### 2.3.2. Electronic Structure of the Pseudo-κ″-(BDH-TTP)$_3$(ReO$_4$)$_2$ (**3**) Salt

The donor layers of this salt (see Figure 8) contain both dimeric units and single donors with an orthogonal orientation.



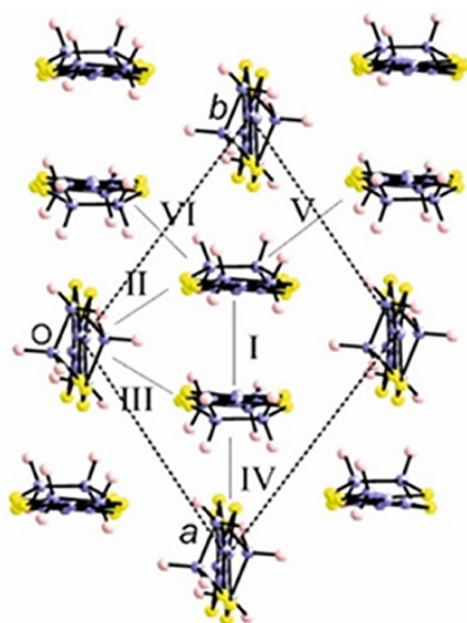**Figure 8.** Donor layer of pseudo-κ″-(BDH-TTP)$_3$(ReO$_4$)$_2$ (**3**) where the different intermolecular interactions are labelled.

The dimeric units form an oblique lattice in the holes of which the single donors reside. The layer contains six different HOMO . . . HOMO interactions of three different types: (i) an intradimer interaction (I), (ii) three different interactions between one donor of the dimer and the single donors (II-IV), and (iii) two different interactions between donors of the dimeric units (V-VI). The calculated HOMO . . . HOMO interaction energies are: 0.7480 eV (I), 0.1190 eV (II), 0.1992 eV (III), 0.0585 eV (IV), 0.1260 eV (V) and 0.2431 eV (VI). The intra-dimer interaction is thus very strong and it will lead to bonding and antibonding combinations of the two HOMOs separated by a large energy gap. Because of the 3:2 stoichiometry, only one of the two levels will be filled since the HOMO of the single donor will be located within this energy gap. Thus, the single donor must be considered as neutral and the two donors of the dimer as positively charged despite the apparent similarity in C=C bond lengths. Note, however, that the C=C distances are shorter in the single donor (1.345/1.362/1.345 Å in the single donor versus 1.365/1.374/1.365 Å in the dimers), and this fact is consistent with the presence of both neutral and singly charge donor molecules.

The interactions between the two different types of molecule (interactions II to IV) are smaller but quite substantial because several S . . . S contacts are relatively short.

Finally, the HOMO ... HOMO interactions between donors of the dimers (V-VI) are calculated to be very substantial, especially for the interactions approximately along the *a* direction. The calculated band structure is shown in Figure 9. As expected, the upper and lower bands are built from the antibonding and bonding combinations of the two HOMOs of the dimeric units. In between the two bands there is a third band based on the HOMO of the single molecule. This is the highest occupied band of the system which is considerably less dispersive. Note that the upper, empty band in Figure 9 exhibits a quite substantial energy dispersion of ~0.4 eV, although the dispersion along the *a*-direction is approximately twice as large as that along the *b*-direction, in agreement with the analysis of the different interactions.
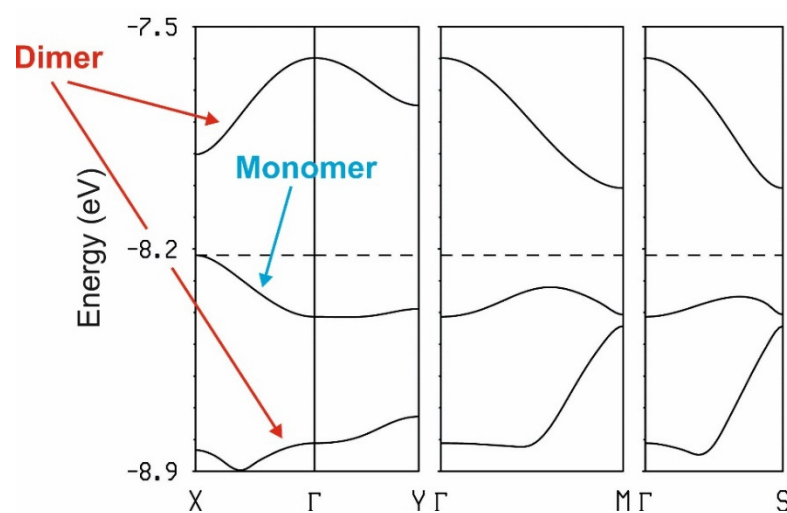


**Figure 9.** Calculated band structure for the donor layers of pseudo-κ''-(BDH-TTP)$_3$(ReO$_4$)$_2$ (**3**) crystals. The dashed line refers to highest occupied level and $\Gamma = (0, 0)$, $X = (a^*/2, 0)$, $Y = (0, b^*/2)$, $M = (a^*/2, b^*/2)$ and $S = (-a^*/2, b^*/2)$.

Thus, this salt must be an anisotropic semiconductor with an indirect gap from X to M and better conductivity along a direction between *a* and *a* + *b*, since both holes and electrons have smaller effective masses along these directions. The calculated activation energy is 105 meV.

*2.4. Conductivity and Magnetic Properties*

2.4.1. Conducting Properties of the κ-(BDH-TTP)$_4$ReF$_6$ (**1**) and κ-(BDH-TTP)$_4$ReF$_6$·4.8H$_2$O (**2**) Crystals

Crystals of **1** and **2** were first characterized by resistance measurements at ambient pressure and pressure up to 10 kbar. At room temperature, the ambient pressure conductivity of crystals of **1** and **2** is 3–5 and 8–10 Ohm$^{-1}$ cm$^{-1}$, respectively. Figure 10a,b shows the temperature dependences of the resistivity of the crystal of **1** measured both in the conducting plane of the BDH-TTP radical cation layers and in the perpendicular direction. As one can see from Figure 10, in both directions at ambient pressure and, under the pressure, the sample shows a metallic behavior of the resistivity with a significant drop at 300–50 °C and a weak growth of the resistivity at lower temperatures, probably due to the localization of carriers resulting from the disorder in the crystal structure of the salt.
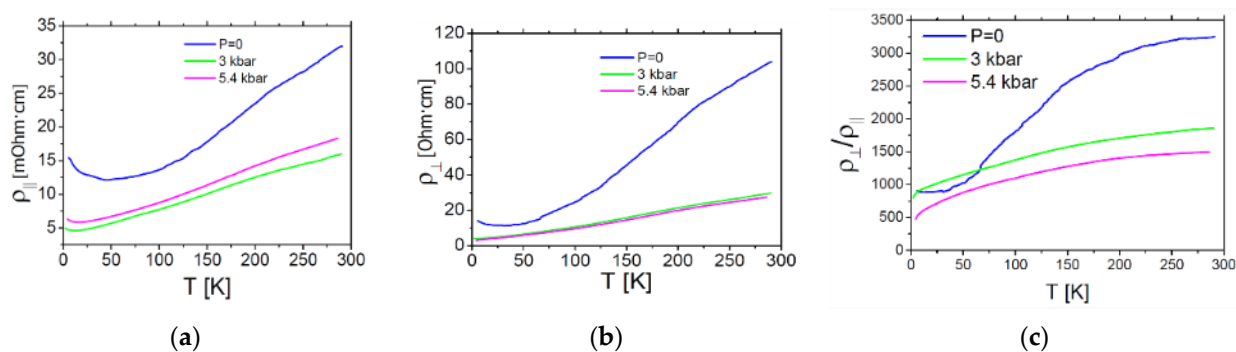
**Figure 10.** (**a**) Temperature dependence of the resistivity of the κ-(BDH-TTP)$_4$ReF$_6$ sample (**1**) measured in the conducting plane and (**b**) perpendicular to it at different pressures; (**c**)The temperature dependence of the resistivity anisotropy of (**1**).

Under external pressures of 3 and 5 kbar, the crystal's resistivity also exhibits a metallic behavior but no transition toward a superconducting state was observed. Interestingly, the growth of the conductivity with decreasing temperature is stronger in the direction perpendicular to the conducting layers. The dependence of the resistivity anisotropy with temperature and pressure is presented in Figure 10c. The room-temperature anisotropy of the resistivity at ambient pressure is approximately 3300. When the temperature drops to 4.2 K, it falls about 3.5 times. When external pressure is applied (in the range from 3 to 5.4 kbar), the anisotropy decreases but depends weakly on the pressure, while a decrease in the temperature from 300 to 4.2 K contributes to its decrease by about 2.3 times.

The crystal of **2** shows a metallic behavior in the 300–4.2 K temperature range at ambient pressure as well as under 1 kbar along the conducting plane (see Figure 11). At ambient pressure, the sample resistance is significantly reduced with the temperature. Under the pressure P = 1 kbar a monotonous and considerable drop in the resistance is observed in the 300–50 K temperature range. However, with a further decrease in the temperature, the drop of the resistance flattens. The metallic character of the conductivity of salts **1** and **2** correlates well with the calculations of their electronic structures (see Section 2.3).
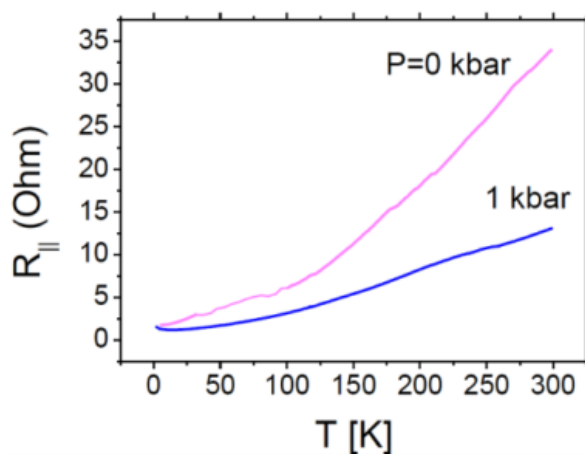


**Figure 11.** The temperature and pressure dependencies of the resistance measured in the conducting *bc* plane at P = 0 kbar and **1** kbar of the κ-(BDH-TTP)$_4$ReF$_6$·4.8H$_2$O (**2**) crystals.

### 2.4.2. Conductivity of the Pseudo-κ''-(BDH-TTP)$_3$(ReO$_4$)$_2$ (**3**) Crystals

The room temperature conductivity of crystals of **3** measured in the plane of the conducting layers is ≈1–1.5 Ohm$^{-1}$ cm$^{-1}$. With the temperature decrease (Figure 12), the sample shows an exponential dependence of the resistivity with an activation energy equal to 0.11 eV, which correlates well with the value of the activation energy obtained from calculations of the electronic band structure of this salt. It should be noted that the sample conductivity value is quite high in comparison with that of typical organic semiconductors.

Looking at the band structure of **3** (Figure 9), it is clear that both the top of the middle band (occupied and centered on the single molecules) and, especially, the bottom of the upper band (empty and centered on the dimers), exhibit a significant energy variation, that is, a relatively low effective mass. Thus, both the electron and hole carriers have small effective masses due to the strong intermolecular interactions and are likely responsible for the high conductivity even if the salt exhibits an activated conductivity.
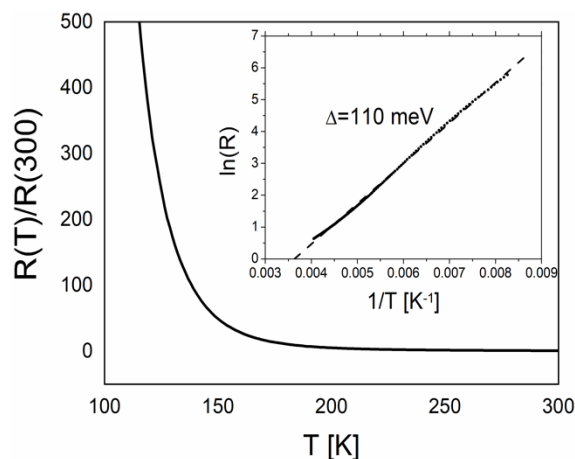


**Figure 12.** The temperature and pressure dependence of the resistance of the pseudo-$\kappa''$-(BDH-TTP)$_3$(ReO$_4$)$_2$ (**3**) salt measured in the conducting *ab* plane.

### 2.4.3. *ac*- Magnetic Properties of the $\kappa$-(BDH-TTP)$_4$[ReF$_6$] Salt (**1**)

In order to test whether the anion of [ReF$_6$]$^{2-}$ as a counterion in the radical cation salt $\kappa$-(BDH-TTP)$_4$[ReF$_6$] retains the properties of single ion magnet (SIM), we have investigated the ac magnetic susceptibility of **1** at 2 K under zero applied *dc* field and different *dc* fields (0–0.6 Tesla). Within the frequency range 10–10,000 Hz, compound **1** does not show a signal for out-of-phase magnetic susceptibility ($\chi''$) under zero applied *dc* field. The maximum of $\chi''$ is not observed on either the field dependence of $\chi''$ at a frequency of 100 Hz or on the frequency dependence of $\chi''$ in a field of 0.4 Tesla; the $\chi''$ signal hovers around 0 (Figure S8, Supplementary Materials). The presence of maxima in the frequency or field dependences of $\chi''$ indicates a slow relaxation of the magnetization, which is one of the distinctive features of SMMs [7–11]. Thus, the study of the *ac* susceptibility of salt **1** shows that this compound is not an SMM, unlike the parent complex (PPh$_4$)$_2$[ReF$_6$]·2H$_2$O [15] and the organic metal (BEDO)$_4$[ReF$_6$]·6H$_2$O [16]. The loss of SIM properties by the anion [ReF$_6$]$^{2-}$ in the composition of salt **1** is possibly associated with the presence of greater disorder in the structure of the anionic layers in crystals of **1**.

### 3. Materials and Methods

All solvents were obtained, chemically clean or extremely clean, from Merk-Sigma-Aldrich and have been used without further purification. The donor BDH-TTP was synthesized according to the method described in [21] and was recrystallized from CS$_2$ (carbon disulfide). The electrolyte (PPh$_4$)$_2$[ReF$_6$]·2H$_2$O was prepared according to the procedure described in [15].

### *3.1. Synthesis of the Salts*

#### 3.1.1. Synthesis of the Crystals $\kappa$-(BDH-TTP)$_4$ReF$_6$ (**1**)

The rhombus-shaped crystals of **1** were prepared under argon atmosphere by electrochemical oxidation of BDH-TTP (C$_1$ = 8 mg, 0.021·10$^{-3}$ mmol) in the presence of the supporting electrolyte (PPh$_4$)$_2$[ReF$_6$]·2H$_2$O (C$_2$ = 21 mg, 0.028 mmol) in a chlorobenzene (CB, 18 mL)–trifluoroethanol (2 mL) mixture. The reaction was performed at constant current, I = 1.25 μA, at 25 K. The synthesis was carried out in an H-shaped two-electrode

glass cell with cathodic and anodic chambers separated by a porous glass membrane. The electrodes were 1 mm diameter platinum wires, electrochemically purified in a 0.1 N sulfuric acid solution. The crystals of **1** formed on the anode within 7–10 days. Electron-probe X-ray microanalysis (EPMA) showed a ratio of S: Re: F atoms to be $\cong$ 33.1:1:6.2.

### 3.1.2. Synthesis of the Crystals κ-(BDH-TTP)$_4$ReF$_6$·4.8H$_2$O (**2**) and Pseudo-κ"-(BDH-TTP)$_3$(ReO$_4$)$_2$ (**3**)

The rhombic crystals of **2** and plate-like crystals of **3** were prepared under argon atmosphere by electrochemical oxidation of BDH-TTP. Unlike the synthesis procedure for crystals **1**, a mixture of chlorobenzene (CB, 18 mL)–96% alcohol (2 mL) was used as the reaction medium. The crystals of **2** and **3** were formed simultaneously on the anode within three weeks.

A preliminary analysis of the crystal compositions determined by electron-probe X-ray microanalysis (EPMA) showed a ratio of S:Re:F and S:Re:O atoms $\cong$ 33.9:1:6.7 and $\cong$ 23.5:1:3.7 for rhombic and plate-like crystals, respectively. The final composition of crystals of **2** and **3** was established from complete X-ray diffraction analysis.

### *3.2. Electron-Probe X-ray Microanalysis*

Preliminary composition of the salts was determined with the electron-probe X-ray microanalysis (EPMA) on a JEOL JSM-5800L scanning electron microscope (SEM) at 100-fold magnification and 20 keV electron beam density. The depth of beam penetration into the sample was 1–3 μm.

### *3.3. Single Crystal X-ray Analysis*

X-ray diffraction analyses of the salts **1**–**3** were carried out on a CCD Agilent XCalibur diffractometer with an EOS detector (Agilent Technologies UK Ltd., Yarnton, Oxfordshire, England). Data collection, determination and refinement of unit cell parameters were carried out using the CrysAlis PRO program suite [26]. X-ray diffraction data at 150(1) K or 100(1) K for the salts **1**–**2** and **3**, respectively, were collected using MoKα (λ = 0.71073 Å) radiation.

The structure (**1**) was solved by the direct methods. The positions and thermal parameters of non-hydrogen atoms were refined isotropically and then anisotropically by the full-matrix least-squares method. At the first stages, the atomic population of the [ReF$_6$]$^{2-}$ anion was refined; at latter stages it was fixed. The positions of the hydrogen atoms were calculated geometrically.

The structure (**2**) was solved with the direct methods. The positions and thermal parameters of non-hydrogen atoms were refined isotropically and then anisotropically by the full-matrix least-squares method. The anion was found to be disordered over two positions; the refinement was carried out, imposing restrictions on bond lengths and thermal parameters. In difference syntheses of the electron density near the Re positions, peaks of the electron density were revealed; they were taken as disordered water atoms. Taking these peaks into account made it possible to improve the refinement of the structure by about 3%. In the first stages, the population of the anion and water molecules was refined and during the final refinement it was fixed. The positions of the hydrogen atoms were calculated geometrically.

The structure of **3** was solved by the direct methods. The positions and thermal parameters of non-hydrogen atoms were refined isotropically and then anisotropically by the full-matrix least-squares method. Oxygen atoms in the tetrahedron, disordered over two positions, were refined with restrictions imposed on bond lengths, position populations and thermal parameters.

The X-ray crystal structures data have been deposited with the Cambridge Crystallographic Data Center, with reference codes CCDC 2069204–2069206. Selected crystallographic parameters and the data collection and refinement statistics are given in Table S1. All calculations were performed with the SHELX-97 program package [27].

### 3.4. Band Structure Analysis

The tight-binding band structure calculations were of the extended Hückel type [28]. A modified Wolfsberg-Helmholtz formula was used to calculate the non-diagonal $H_{\mu\nu}$ values [29]. All valence electrons were taken into account in the calculations and the basis set consisted of Slater-type orbitals of double-$\zeta$ quality for C 2s and 2p, S 3s and 3p, and of single-$\zeta$ quality for H. The ionization potentials, contraction coefficients and exponents were taken from previous work [30]. The possible role of the disorder of the terminal ethylene groups was checked by carrying out calculations with different combinations of the major and minor configurations. As it is generally found, there was no effect on the results because the HOMO does not exhibit a noticeable contribution of these terminal ethylene groups.

### 3.5. Conducting Properties

Resistivity measurements were carried out using a four-probe technique and a lock-in amplifier at 20 Hz alternating current. The samples were thin plates with a characteristic lateral size of about 0.4–1 mm and the thickness was in the range 15–50 μm. The surface of the plate was oriented along the conducting layers, that is, parallel to the (*bc*) plane. Depending on the size and the shape of the samples, we could measure either in-plane resistance or resistances in both in-plane and out-of-plane directions. The first case concerns the samples of crystals of **2** and **3,** which were thin and comparatively long plates, so we could make four contacts along one of the sample's surfaces and measure the in-plane resistance. As for the samples of crystals of **1**, we could make two contacts, attached to each of two opposite sample surfaces and measured both in-plane $R_{||}$ and out-of-plane $R_{\perp}$ resistances and calculated the resistivity using the modified Montgomery method [31]. The contacts were made using the conducting graphite paste. The measurements in the 1.3–300 K temperature range were carried out in a $^4$He cryostat with a variable temperature insert. To create an external pressure of up to 5.4 kbar, the samples were subjected to quasi-hydrostatic pressure using a Cu-Be clamp-cell with silicone oil as a pressurized medium and a manganin sensor for pressure control.

### 3.6. Magnetic Properties

Alternating-current (*ac*) magnetic susceptibility measurements were performed on the polycrystalline sample of salt **1** using a PPMS magnetometer (Quantum Design) under an *ac* field of 3 Oe. The data were collected in a zero *dc* field and different applied *dc* fields.

### 4. Conclusions

Three new radical cation salts: κ-(BDH-TTP)$_4$ReF$_6$ (**1**), κ-(BDH-TTP)$_4$ReF$_6$·4.8H$_2$O (**2**) and pseudo-κ''-(BDH-TTP)$_3$[ReO$_4$]$_2$ (**3**) have been obtained with original electrocrystallization methods using various mixtures of solvents and electrolyte (PPh)$_2$[ReF$_6$]·2H$_2$O that is field-induced SIM. The addition of rectified (96%) ethanol and trifluoroethanol to chlorobenzene as the main solvent is critical for the formation of these salts. Crystals of salt **1** are formed if trifluoroethanol is used, while the addition of 96% ethanol leads to partial oxidation of paramagnetic Re(IV) to diamagnetic Re(VII) during the electrocrystallization, resulting in the formation of salts **2** and **3.**

The radical cation salts are characterized by the alternation of layers of organic radical cations with layers composed of isolated anions [ReF$_6$]$^{2-}$, [ReF$_6$]$^{2-}$·4.8H$_2$O and [ReO$_4$]$^-$ for salts **1**, **2** and **3,** respectively. In compounds **1** and **2**, the radical cation layers have the κ-type of molecular packing formed by BDH-TTP equivalent dimers, while in **3**, the organic layers consist of radical cation dimers (BDH-TTP)$_2^{2+}$ and single molecules BDH-TTP (a new type of pseudo-κ''-packing). A distinctive feature of these salts is the occurrence of disorder in the anionic layers and incomplete population of the Re anions in the crystalline lattice.

The study of the temperature dependences of the conductivity for salts **1**–**3** shows that **1** and **2** are stable molecular metals, and **3** is a semiconductor with a conductivity activation energy of 110 meV. Calculations of the electronic band structures of the salts correlate well

with the data on conductivity measurements. The Fermi surface of **1** and **2** contains closed circuits with areas of 100% and approximately 17% of the cross section of the Brillouin zone. The band structure of **3** clearly shows that this salt should be a semiconductor with high enough conductivity and that in the salt crystal structure the single donors must be considered as neutral molecules and the dimers as $(BDH\text{-}TTP)_2^{2+}$.

Analysis of the *ac* magnetic susceptibility of salt **1** shows that this compound does not exhibits the properties of SMMs, which could be expected from the presence of the $[ReF_6]^{2-}$ anion in the composition of salt. Perhaps this is due to the presence of significant disorder in the structure of the anionic layers in crystals **1**.

**Supplementary Materials:** The following are available online at https://www.mdpi.com/article/10.3390/magnetochemistry7040054/s1, Figure S1: Asymmetric unit and the designations of the radical cation and anion in the crystals κ-$(BDH\text{-}TTP)_4ReF_6$ salt (**1**); Figure S2. Mutual arrangement of the radical cations in the dimer and the designations of central C=C bond in the molecules κ-$(BDH\text{-}TTP)_4ReF_6$ salt (**1**); Figure S3. Asymmetric unit and the designations of the radical cation and anion in the crystals κ-$(BDH\text{-}TTP)_4ReF_6 \cdot 4.8H_2O$ (**2**); Figure S4. Mutual arrangement of the radical cations in the dimer and the designations of central C=C bond in the molecules κ-$(BDH\text{-}TTP)_4ReF_6 \cdot 4.8H_2O$ salt (**2**); Figure S5. Asymmetric unit and the designations of the radical cations and anion in the crystals pseudo-κ"-$(BDH\text{-}TTP)_3(ReO_4)_2$ (**3**); Figure S6. Mutual arrangement of the radical cations in the dimer and the designations of central C=C bond in the molecules of the pseudo-κ"-$(BDH\text{-}TTP)_3([ReO_4]_2$ salt (**3**). Dashed lines show shortened contacts designated as S2 . . . S6 and S3 . . . S7 between the radical cation in the dimer; Figure S7. The short contacts between the radical cation inside the dimer and between the dimer and single BDH-TTP molecules; Figure S8. Frequency dependences of the out-of-phase ($\chi''$) ac susceptibility for κ-$(BDH\text{-}TTP)_4ReF_6$ salt (**1**) at temperature of 2.0 K in a dc field of 0.4 Tesla; Table S1. Crystallographic data and refined structural parameters for the crystals **1–3**; Table S2. Bond length of Re=O in a tetrahedron $[ReO_4]^-$.

**Author Contributions:** Data curation, N.D.K., G.V.S., L.I.B., V.N.Z., E.C. and J.-i.Y.; Formal analysis, N.D.K., G.V.S., L.I.B., V.N.Z., E.C. and J.-i.Y.; Investigation, G.V.S., L.I.B., E.B.Y., V.N.Z., E.C. and J.-i.Y.; Project administration, E.B.Y.; Writing—original draft, N.D.K., G.V.S., L.I.B. and E.B.Y.; Writing—review & editing, G.V.S., L.I.B. and E.B.Y. All authors have read and agreed to the published version of the manuscript.

**Conflicts of Interest:** The authors declare no conflict of interest. The funders had no role in the design of the study; in the collection, analyses, or interpretation of data; in the writing of the manuscript, or in the decision to publish the results.

## References

1. Ouahab, L. *Multifunctional Molecular Materials*, 1st ed.; Pan Stanford Publishing Pte. Ltd.: Singapore, 2013.
2. Coronado, E.; Day, P. Magnetic Molecular Conductors. *Chem. Rev.* **2004**, *104*, 5419–5449. [CrossRef] [PubMed]
3. Kobayashi, H.; Cui, H.; Kobayashi, A. Organic Metals and Superconductors Based on BETS (BETS = Bis(ethylenedithio)-tetraselenafulvalene. *Chem. Rev.* **2004**, *104*, 5265–5288. [CrossRef] [PubMed]
4. Kushch, N.D.; Yagubskii, E.B.; Kartsovnik, M.V.; Buravov, L.I.; Dubrovskii, A.D.; Chekhlov, A.N.; Biberacher, W. π-donor BETS Based Bifunctional Superconductor with Polymeric Dicyanamidomanganate(II) Anion Layer: κ-$(BETS)_2Mn[N(CN)_2]_3$. *J. Am. Chem. Soc.* **2008**, *130*, 7238–7240. [CrossRef] [PubMed]
5. Prokhorova, T.G.; Yagubskii, E.B. Organic Conductors and Superconductors Based on Bis(ethylenedithio)tetrathia-fulvalene Radical Cation Salts with Supramolecular Tris(oxalato)metallate Anions. *Russ. Chem. Rev.* **2017**, *86*, 164–180. [CrossRef]
6. Cosquer, G.; Shen, Y.; Almeida, M.; Yamashita, M. Conducting Single-molecule Magnet Materials. *Dalton Trans.* **2018**, *47*, 7616–7627. [CrossRef]
7. Gatteschi, D.; Sessoli, R.; Villain, J. *Molecular Nanomagnets, Mesoscopic Physics and Nanotechnology*; Oxford University Press: Oxford, UK, 2006.

8.  Milios, C.; Winpenny, R.E.P. Cluster-Based Single-Molecule Magnets. In *Structure and Bonding*; Gao, S., Ed.; Springer: Berlin/Heildelberg, Germany, 2015; Volume 164, pp. 1–109.

9.  Bogani, L.; Wernsdorfer, W. Molecular Spintronics Using Single-molecule Magnets. *Nature Mater.* **2008**, *7*, 179–186. [CrossRef]

10. Aromi, G.; Aguilà, D.; Gamez, P.; Luis, F.; Roubeau, O. Molecules as Prototypes for Spin-Based CNOT and SWAP Quantum Gates. *Chem. Soc. Rev.* **2012**, *41*, 537–546.

11. Bartolomé, J.; Luis, F.; Fernandez, J. *Molecular Magnets–Physics and Applications*; Springer: Berlin/Heidelberg, Germany, 2014.

12. Kubo, K.; Hiraga, H.; Miyasaka, H.; Yamashita, M. Multifunctional Single-molecule Magnets with Electrical Conductivity. In *Multifunctional Molecular Materials*; Ouahab, L., Ed.; Pan Stanford Publishing Pte. Ltd.: Singapore, 2013; pp. 61–103.

13. Zhang, X.; Xie, H.; Ballesteros-Rivas, M.; Woods, T.J.; Dunbar, K.R. Conducting Molecular Nanomagnet of Dy(III) with Partially Charged TCNQ Radicals. *Chem. Eur. J.* **2017**, *23*, 7448–7452. [CrossRef]

14. Shen, Y.; Cosquer, G.B.; Breedlove, K.; Yamashita, M. Hybrid Molecular Compound Exhibiting Slow Magnetic Relaxation and Electrical Conductivity. *Magnetochemistry* **2016**, *2*, 44. [CrossRef]

15. Pedersen, K.S.; Sigrist, M.; Sorensen, M.A.; Barra, A.-L.; Weyhermuller, T.; Piligkos, S.; Thuesen, C.A.; Vinum, M.G.; Mutka, H.; Weihe, H.; et al. $[ReF_6]^{2-}$: A Robust Module for the Design of Molecule-Based Magnetic Materials. *Angew. Chem. Int. Ed.* **2014**, *53*, 1351–1354. [CrossRef]

16. Kushch, N.D.; Buravov, L.I.; Kushch, P.P.; Shilov, G.V.; Yamochi, H.; Ishikawa, M.; Otsuka, A.; Shakin, A.; Maximova, O.V.; Volkova, O.S.; et al. The Multifunctional Compound Combining Conductivity and Single-Molecule Magnetism in the Same Temperature Range. *Inorg. Chem.* **2018**, *57*, 2386–2389. [CrossRef]

17. Shen, Y.; Ito, H.; Zhang, H.; Yamochi, H.; Katagiri, S.; Yoshina, S.K.; Otsuka, A.; Ishikawa, M.; Cosquer, G.; Uchida, K.; et al. Simultaneous Manifestations of Metallic Conductivity and Single-Molecule Magnetism in a Layered Molecule-based Compound. *Chem. Sci.* **2020**, *11*, 11154–11161. [CrossRef]

18. Yamada, J.-I.; Akutsu, H.; Nishikawa, H.; Kikuchi, K. New Trends in the Synthesis of $\pi$-Electron Donors for Molecular Conductors and Supercondutors. *Chem. Rev.* **2004**, *104*, 5057–5083. [CrossRef] [PubMed]

19. Bardin, A.; Akutsu, H.; Yamada, J.-I. New Family of Six Stable Metals with a Nearly Isotropic Triangular Lattice of Organic Radical Cations and Diluted Paramagnetic System of Anions: $\kappa(\kappa_\perp)$-(BDH-TTP)$_4$MX$_4$·Solv, Where M = Co$^{II}$, Mn$^{II}$.; X = Cl, Br and Solv = (H$_2$O)$_5$, (CH$_2$X). *Cryst. Growth Des.* **2016**, *16*, 1228–1246. [CrossRef]

20. Williams, J.M.; Ferraro, R.J.; Thorn, R.J.; Carlson, K.D.; Geiser, U.; Wang, H.H.; Kini, A.M.; Whangbo, M.-H. *Organic Superconductors (Including Fullerenes)*; Prentice Hall, Englewood Cliffs: New Jersey, NJ, USA, 1992.

21. Yamada, J.; Watanabe, M.; Anzai, H.; Nishikawa, H.; Ikemoto, I.; Kikuchi, K. BDH-TTP as a Structural Isomer of BEDT-TTF, and Its Two-Dimensional Hexafluorophosphate Salt. *Angew. Chem. Int. Ed.* **1999**, *38*, 810–813. [CrossRef]

22. Kurmoo, M.; Graham, A.W.; Day, P.; Coles, S.J.; Hursthouse, M.B.; Caulfield, J.L.; Singleton, J.; Pratt, F.L.; Hayes, W.; Ducasse, L.; et al. Superconducting and Semiconducting Magnetic Charge Transfer Salts: (BEDT-TTF)$_4$AFe(C$_2$O$_4$)$_3$·C$_6$H$_5$CN (A = H$_2$O, K, NH$_4$). *J. Am. Chem. Soc.* **1995**, *49*, 12209–12217. [CrossRef]

23. Whangbo, M.H.; Williams, J.M.; Leung, P.C.W.; Beno, M.A.; Emge, T.J.; Wang, H.H. Role of the Intermolecular Interactions in the Two-Dimensional Ambient-Pressure Organic Superconductors $\beta$-(ET)$_2$I$_3$ and $\beta$-(ET)$_2$IBr$_2$. *Inorg. Chem.* **1985**, *24*, 3500–3502. [CrossRef]

24. Shevyakova, I.; Buravov, L.; Tkacheva, V.; Zorina, L.; Khasanov, S.; Simonov, S.; Yamada, J.; Canadell, E.; Shibaeva, R.; Yagubskii, E. New Organic Metals Based on BDH-TTP Radical Cation Salts with the Photochromic Nitroprusside Anion [FeNO(CN)$_5$]$^{2-}$. *Adv. Funct. Mater.* **2004**, *14*, 660–668. [CrossRef]

25. Kushch, N.D.; Kazakova, A.V.; Buravov, L.I.; Yagubskii, E.B.; Simonov, S.V.; Zorina, L.V.; Khasanov, S.S.; Shibaeva, R.P.; Canadell, E.; Son, H.; et al. The First BDH-TTP Radical Cation Salts with Mercuric Counterions, $\kappa$-(BDH-TTP)$_4$[Hg(SCN)$_4$]C$_6$H$_5$NO$_2$ and $\kappa$-(BDH-TTP)$_6$[Hg(SCN)$_3$][Hg(SCN)$_4$] . *Synth. Met.* **2005**, *155*, 588–594. [CrossRef]

26. Agilent. *CrysAlis PRO Version171.35.19*; Agilent Technologies UK Ltd.: Yarnton, Oxfordshire, UK, 2011.

27. Sheldrick, G.M. *SHELXL-97. Program for Crystal Structure Refinement*; University of Göttingen: Göttingen, Germany, 1997.

28. Whangbo, M.H.; Hoffmann, R. The Band Structure of the Tetracyanoplatinate Chain. *J. Am. Chem. Soc.* **1978**, *100*, 6093–6098. [CrossRef]

29. Ammeter, J.H.; Buergi, H.B.; Thibeault, J.C.; Hoffmann, R. Counterintuitive Orbital Mixing in Semiempirical and ab initio Molecular Orbital Calculations. *J. Am. Chem. Soc.* **1978**, *100*, 3686–3692. [CrossRef]

30. Penicaud, A.; Boubekeur, K.; Batail, P.; Canadell, E.; Auban-Senzier, P.; Jerome, D. Hydrogen-bond Tuning of Macroscopic Transport Properties from the Neutral Molecular Component Site along the Series of Metallic Organic-inorganic Solvates (BEDT-TTF)$_4$Re$_6$Se$_5$C$_{I9}$·[G], [Gt = DMF, THF, dioxane]. *J. Am. Chem. Soc.* **1993**, *115*, 4101–4112. [CrossRef]

31. Buravov, L.I. Calculation of Resistance Anisotropy with Allowance for the Ends of the Sample with the Help of a Conformal Transformation. *Sov. Phys. Tech. Phys.* **1989**, *34*, 464–469.